MULTI-TARGET TRACKING USING MULTI-MODAL SENSING WITH WAVEFORM CONFIGURATION

Jun Jason Zhang[†], Antonia Papandreou-Suppappola[†], and Muralidhar Rangaswamy[‡]

[†]SenSIP Center, School of ECEE, Arizona State University, Tempe, AZ
[‡] Air Force Research Laboratory, Sensors Directorate, Hanscom Air Force Base, MA

ABSTRACT

We investigated the joint multi-modal operation of the asymmetric character of the fields of view of radar and electro optical (EO) sensors for multi-target tracking applications. We proposed a joint multi-modal sensing mode based on using dynamic agility selection to optimize the tracking performance of multiple maneuvering targets. The proposed method jointly designs waveforms for radar sensing and resolution switching modes for EO sensing, when both sensor measurements experience high false alarm rates. Rao-Blackwellized particle filtering is used to track an unknown number of targets within an adaptive framework that yields the optimized joint sensor configuration. We demonstrated the performance of the proposed adaptive tracking system using numerical simulations.

Index Terms— Multi-modal sensing, multiple target tracking, Rao-Blackwellized particle filter, waveform-agile sensing.

1. INTRODUCTION

When complementary information from different types of sensors is appropriately combined, the application-specific performance is expected to increase when compared to each sensor's performance separately. For joint dynamic target tracking (using active radio frequency (RF) radar sensors) and target identification (using passive EO sensors), the combined sensor capabilities have the potential of improving the performance over either sensor capability. For example, the kinematic features for target tracking from the RF sensor and the physical features for target identification from the EO sensor can be combined to increase the joint target tracking performance.

When radar and EO sensors were initially integrated (see, for example, [1]), the radar was operated in an imaging mode as a synthetic aperture radar or SAR and thus the targets were stationary. With both the radar and EO sensors providing images, the processing extracted and fused features from both sensor measurements for image identification. In [2], a multi-mode sensing operation was introduced where non-imaging RF and imaging EO measurements were used in a land surveillance application to observe a person walking over a period of time. This type of asymmetric mode sensing resulted in enhanced classification results and reduced number of false alarms. More recently, RF and EO sensors were also jointly used in similar multi sensing modalities to track and characterize human motion based on measuring the walking structure and gait of a person using an imaging approach [3]. Note that other types of sensing modes were also formulated in the literature; for example, for

coupled tracking using three different measurements: ground moving target indicator (GMTI), high-range resolution radar (HRRR), and digital terrain elevation data (DTED) [4]. Asymmetric sensor modalities also need to be investigated to track multiple targets over a wide field of view (FOV). Furthermore, to increase the joint sensing performance and exploit the multi-modality formulation, radar waveform parameters and EO resolution parameters can be independently and adaptively configured.

We consider multi-modal sensing measurements from pulsed-Doppler (PD) radar and EO sensors for tracking multiple targets. This is an attractive sensor combination [2, 5] as the radar provides range and range-rate measurements to detect targets with radial velocity and the EO sensor provides azimuth and elevation angles information to detect stationary targets. When measurements from both sensors are combined, the probability of false alarm and probability of miss-detection are expected to decrease. The multi-modal sensor multi-target tracking problem assumes multiple RF-EO systems, and it has real-life applications. One such example is many unmanned aerial vehicles (UAVs) acting together as a swarm to survey a region and track multiple targets. Each UAV can be equipped with a joint RF-EO sensor system and work independently to send multiple target measurements to a ground data processing center.

We solve the tracker of an unknown number of targets using the Rao-Blackwellized particle filter (RBPF) algorithm [6, 7]. The formulation includes probabilistic stochastic process models for target states, data associations, and target birth/death processes based on sequential Monte Carlo (MC) sampling techniques. The use of the RBPF improves the efficiency of the MC sampling as it results in a largely reduced number of particles and thus in an efficient implementation of the state distribution and measurement likelihood. We develop a waveform-agile multi-modal (WAMM) method to improve the system tracking performance. This is achieved by adaptively selecting waveform and resolution parameters for the radar and EO sensors, respectively, to minimize the joint tracking error.

The rest of the paper is organized as follows. Sections 2 and 3 provide the state and RF/EO measurement models. The joint multi-target multi-modal tracking is derived in Section 4 and with waveform agility in Section 5. Numerical simulations successfully demonstrate the new approach in Section 6.

2. MULTIPLE TARGET TRACKING MODEL

We use a non-maneuvering model to describe a point target moving in a three-dimensional (3-D) space. The state vector representing the position (x_k, y_k, z_k) and velocity $(\dot{x}_k\ \dot{y}_k\ \dot{z}_k)$ Cartesian coordinates of a point target at time step k is given by

$$\mathbf{x}_k = [x_k\ \dot{x}_k\ y_k\ \dot{y}_k\ z_k\ \dot{z}_k]^T, \tag{1}$$

where T denotes vector transpose. The state equation is given by

$$\mathbf{x}_{k+1} = \mathbf{F}\,\mathbf{x}_k + \mathbf{w}_k, \tag{2}$$

where $\mathbf{F} = \mathrm{diag}\{\mathbf{F}_s, \mathbf{F}_s, \mathbf{F}_s\}$, $\mathbf{F}_s$ is a 2×2 matrix with elements $[\mathbf{F}_s]_{11} = [\mathbf{F}_s]_{22} = 1$, $[\mathbf{F}_s]_{21} = 0$, and $[\mathbf{F}_s]_{12} = T_d$, T_d is the duration between time steps, $\mathbf{w}_k$ is a modeling error process with covariance matrix $\mathbf{Q}_k = \mathrm{diag}\{q_{x,k}\mathbf{Q}_s, q_{y,k}\mathbf{Q}_s, q_{z,k}\mathbf{Q}_s\}$, $\mathbf{Q}_s$ is a 2×2 matrix with elements $[\mathbf{Q}_s]_{12} = [\mathbf{Q}_s]_{21} = T_d^2/2$, $[\mathbf{Q}_s]_{11} = T_d^3/3$, and $[\mathbf{Q}_s]_{22} = T_d$, and $q_{x,k}$, $q_{y,k}$ and $q_{z,k}$ are the process noise intensities in the 3-D coordinate axis. For simplicity, we assume that the target moves in the (x, y) horizontal plane, such that $z_k = \dot{z}_k = 0$ in Equation (1). If needed, the model can be changed to a more sophisticated maneuvering dynamic model (e.g., acceleration or turning model) to better match the target's characteristics [8].

If we assume that there are M_k targets present in the FOV of interest (or alive targets) at time step k, then the state vector representing the positions and velocities of these targets is given by

$$\chi_k = \left\{ \mathbf{x}_k^{(1)}, \cdots, \mathbf{x}_k^{(\mathrm{M}_k)} \right\} \tag{3}$$

where $\mathbf{x}_k^{(i)}$ can be represented by the single target state formulation in Equations (1) and (2). Note that the time step M_k varies in order to allow for asynchronous measurements, provided that the measurements maintain their original order of observation.

3. TARGET MEASUREMENT MODEL IN CLUTTER

The RF-EO sensor system considered is assumed to consist of multiple heterogeneous and spatially distributed RF-EO sensors that can provide asynchronous measurements. The system can track an unknown number of targets, while taking into consideration that noise and clutter can result in imperfect detection of the multiple targets with false alarm and mis-detection. As a result, we use data association to associate measurements with targets, and we also allow targets to enter the FOV (birth of a target) and leave the FOV (death of a target). Due to the imperfect detection assumption, RF or EO sensor measurements are first matched filtered before thresholding. For both type of sensors, we need to model measurements as correct measurements that originated from true targets, or as undesired measurements that originated from noise or clutter.

3.1. Radar Sensor Measurement Model

Each resolution cell of the RF sensor provides a matched filter output amplitude for detection, and the detected resolution cell also provides a range-Doppler measurement. We assume that at time step k, m_k measurements are detected that are denoted by $\mathbf{z}_k = \{\mathbf{z}_k^j\}_{j=1}^{m_k}$. The jth measurement vector is given by $\mathbf{z}_k^j = [\rho_k^j \;\; \dot{\rho}_k^j]^T$, where ρ_k^j is the range measurement, and $\dot{\rho}_k^j$ is the range-rate measurement. If the jth measurement originated from the true target, then the measurement $\mathbf{z}_k^j$ can be modeled as $\rho_k^j = r_k + \epsilon_k^r$ and $\dot{\rho}_k^j = \dot{r}_k + \epsilon_k^{\dot{r}}$, where $r_k = [(x_k - x_p)^2 + (y_k - y_p)^2 + (z_k - z_p)^2]^{1/2}$, $\dot{r}_k = \dot{x}_k(x_k - x_p)/r_k + \dot{y}_k(y_k - y_p)/r_k$, and (x_p, y_p, z_p) is the sensor location in 3-D coordinates. Also, $\epsilon_k^r \sim \mathcal{N}[0, \sigma_r^2]$ is normally distributed with zero-mean and range measurement noise variance σ_r^2, and $\epsilon_k^{\dot{r}} \sim \mathcal{N}[0, \sigma_{\dot{r}}^2]$ is normally distributed with zero-mean and range-rate measurement noise variance $\sigma_{\dot{r}}^2$. The variances are obtained by $\sigma_r^2 = \nu_r^2/12$, $\sigma_{\dot{r}}^2 = \nu_{\dot{r}}^2/12$ [9], where ν_r and $\nu_{\dot{r}}$ are range and range-rate resolutions, respectively. As a result, the conditional probability density of $\mathbf{z}_k^j$ that results from the true target is given by

$$p_1(\mathbf{z}_k^j | \mathbf{x}_k) = (2\pi\sigma_r\sigma_{\dot{r}})^{-1} \exp\left(-\frac{1}{2}\left(\frac{\rho_k^j - r_k}{\sigma_r}\right)^2 - \frac{1}{2}\left(\frac{\dot{\rho}_k^j - \dot{r}_k}{\sigma_{\dot{r}}}\right)^2 \right)$$

We assume that the false measurements from the false alarms are uniformly distributed in the validation gate volume $V_{\mathrm{RF},k}$. So, if the jth measurement is a false alarm and a rectangular validation gate is used (with volume $V_{\mathrm{RF},k} = \left(r_k^U - r_k^L\right) \times \left(\dot{r}_k^U - \dot{r}_k^L\right)$), then

the measurement $\mathbf{z}_k^j$ can be modeled such that α_k^j follows the density $p_0^\tau(\alpha_k^j)$, $\rho_k^j \sim \mathcal{U}[r_k^L, r_k^U]$, and $\dot{\rho}_k^j \sim \mathcal{U}[\dot{r}_k^L, \dot{r}_k^U]$. Here, $\mathcal{U}[\cdot]$ denotes the uniform distribution, the range ρ_k^j is uniformly distributed between the lower bound r_k^L and upper bound r_k^U of the range validation gate, and the range-rate is similarly distributed between the corresponding bounds $\dot{r}_k^L$ and $\dot{r}_k^U$. As a result, the conditional density of $\mathbf{z}_k^j$ that results from false alarms is given by $p_0(\mathbf{z}_k^j | \mathbf{x}_k) = 1/V_{\mathrm{RF},k}$.

3.2. EO Sensor Measurements

For the EO sensor, the measurements extracted from the optical image are elevation angle and azimuth angle. We assume that at time step k, n_k measurements are detected and denoted by $\mathbf{y}_k = \{\mathbf{y}_k^j\}_{j=1}^{n_k}$ with $\mathbf{y}_k^j = [\phi_k^j \;\; \psi_k^j]^T$, where ϕ_k^j is the elevation angle measurement, and ψ_k^j is the azimuth angle measurement. Following similar steps as for the RF sensor, the conditional density $p_1(\mathbf{y}_k^j | \mathbf{x}_k)$ for measurements resulting from a true target is also a Gaussian density with the elevation and azimuth angles of the true target given by $\theta_k = \sin^{-1}((z_k - z_p)/r_k)$ and $\eta_k = \sin^{-1}((x_k - x_p)/r_k)$. For the EO sensor, σ_θ and σ_η are the standard deviations of the elevation and azimuth angle measurements [9]. The conditional density for measurements resulting from false alarms is given by $p_0(\mathbf{y}_k^j | \mathbf{x}_k) = 1/V_{\mathrm{EO},k}$, where $V_{EO,k}$ is the validation area volume at time step k.

4. JOINT RF-EO MULTI-TARGET TRACKING

The RBPF decomposes a filtering problem that would require MC sampling into two filtering problems: (a) one that can be solved in closed form; and (b) a lower dimensionality one than the original that would require MC sampling but would not be as computationally intensive as the original one. Also, solving some of the equations in closed form instead of using MC sampling for all the equations can be shown to produce estimators with lower variance [6]. Considering a system with state vector $\mathcal{S}_k$ and measurement vector ζ_k at time step k, the state space model can be given by the density functions $p(\mathcal{S}_k | \mathcal{S}_{k-1})$ and $p(\zeta_k | \mathcal{S}_k)$. If we partition the state vector into $\mathcal{S}_k = [\chi_k^T \; \lambda_k^T]^T$, the state space model can be re-written as $p(\chi_k | \chi_{k-1}, \lambda_{k-1}, \lambda_k)$, $p(\lambda_k | \chi_{k-1}, \lambda_{k-1})$, and $p(\zeta_k | \chi_k, \lambda_k)$. If $p(\chi_k | \chi_{k-1}, \lambda_{k-1}, \lambda_k)$ and $p(\zeta_k | \chi_k, \lambda_k)$ can be calculated in closed form, we can apply MC sampling only to λ_k, with λ_k independent of χ_{k-1} so that $p(\lambda_k | \chi_{k-1}, \lambda_{k-1}) = p(\lambda_k | \lambda_{k-1})$. Thus, we can greatly reduce the particle filtering complexity and lead to more accurate estimation results.

For the joint RF-EO multi-target tracking, the state formulation of the M_k alive targets is given in Equation (3). As we assume that, at each time step, the measurement ζ_k has resulted from only one target (or false alarm or new target birth or target death), then before the RBPF partition, the target state can be considered as $\mathcal{S}_k = [\chi_k^T \; \lambda_k^T]^T$, where the vector λ_k represents the events that may happen during tracking. Assuming that at time $k-1$, there are M_{k-1} alive targets, there are $2 \times (1 + \mathrm{M}_{k-1}) + \mathrm{M}_{k-1}^2$ such events that can happen, and λ_k can consist of any of these events with a probability described by $p(\lambda_k | \lambda_{k-1})$. These events include: (a) ζ_k is associated to clutter, and no target dies; (b) ζ_k is associated to clutter, and the jth target dies, $j = 1, \cdots, \mathrm{M}_{k-1}$; (c) ζ_k is associated to the jth target, and no target dies, $j = 1, \cdots, \mathrm{M}_{k-1}$; (d) ζ_k is associated to the jth target, and the ith target dies, $i, j = 1, \cdots, \mathrm{M}_{k-1}$, and $i \neq j$; (e) ζ_k is associated to a new target, and no target dies; (f) ζ_k is associated to a new target, and the jth target dies, $j = 1, \cdots, \mathrm{M}_{k-1}$. Note that we also assume that the prior transfer probability of the events, $p(\lambda_k | \lambda_{k-1})$, is independent of the target states χ_{k-1}. Given the above notation, the RBPF can be implemented by fixing some

parameters such as false alarm rate, target birth probability and target death probability. The main constraint of this algorithm is that it allows only one target birth or death at each time step. A method to overcome this constraint is discussed in [6].

5. WAVEFORM-AGILE MULTI-MODAL DESIGN

5.1. Posterior Cramér-Rao Lower Bound for Target Tracking

We derived the posterior Cramér-Rao lower bound (PCRLB) for tracking a single target using the joint RF-EO sensor system [10]. This result can be extended to the multiple target case when the targets are assumed close together. Let $\hat{\mathbf{x}}_k$ be an unbiased estimate of the target state $\mathbf{x}_k$ using the RF measurements $\mathcal{Z}_k = \{\mathbf{z}_1, \cdots, \mathbf{z}_k\}$, EO measurements $\mathcal{Y}_k = \{\mathbf{y}_1, \cdots, \mathbf{y}_k\}$, and an initial state density $p(\mathbf{x}_0)$. The covariance matrix of $\hat{\mathbf{x}}_k$ has the lower bound

$$\mathbf{P}_k = \mathrm{E}\{(\hat{\mathbf{x}}_k - \mathbf{x}_k)(\hat{\mathbf{x}}_k - \mathbf{x}_k)^T\} \geq \mathbf{J}_k^{-1},$$

where the difference $(\mathbf{P}_k - \mathbf{J}_k^{-1})$ is a positive semi-definite matrix and $\mathbf{J}_k^{-1}$ is the Fisher information matrix whose inverse is the PCRLB. $\mathbf{J}_k$ can be computed recursively as [11]

$$\mathbf{J}_{k+1} = \mathbf{Q}_k + \mathbf{J}_{k+1}^{\mathrm{RF,EO}} - \mathbf{F}^T \mathbf{Q}_k^{-1} (\mathbf{J}_k + \mathbf{F}^T \mathbf{Q}_k^{-1} \mathbf{F})^{-1} (\mathbf{Q}_k^{-1})^T \mathbf{F}. \quad (4)$$

Due to space limitations, the detailed steps of the derivation can be found in [10]. It can be shown that $\mathbf{J}_k^{\mathrm{RF,EO}} = \mathbf{J}_k^{\mathrm{RF}}$ or $\mathbf{J}_k^{\mathrm{RF,EO}} = \mathbf{J}_k^{\mathrm{EO}}$, depending on which type of sensor provides measurements, where

$$\mathbf{J}_k^{\mathrm{RF}} = q^{\mathrm{RF}}(P_\mathrm{D}^{\mathrm{RF}}, P_{\mathrm{FA}}^{\mathrm{RF}}, V_g^{\mathrm{RF}}) \int \left(\frac{1}{\sigma_r^2} [\nabla_{\mathbf{x}_k} r_k(\mathbf{x}_k)][\nabla_{\mathbf{x}_k} r_k(\mathbf{x}_k)]^T \right.$$
$$\left. + \frac{1}{\sigma_{\dot{r}}^2} [\nabla_{\mathbf{x}_k} \dot{r}_k(\mathbf{x}_k)][\nabla_{\mathbf{x}_k} \dot{r}_k(\mathbf{x}_k)]^T \right) p(\mathbf{x}_k) \, d\mathbf{x}_k,$$

$$\mathbf{J}_k^{\mathrm{EO}} = q^{\mathrm{EO}}(P_\mathrm{D}^{\mathrm{EO}}, P_\mathrm{D}^{\mathrm{EO}}, V_g^{\mathrm{EO}}) \int \left(\frac{1}{\sigma_\theta^2} [\nabla_{\mathbf{x}_k} \theta_k(\mathbf{x}_k)][\nabla_{\mathbf{x}_k} \theta_k(\mathbf{x}_k)]^T \right.$$
$$\left. + \frac{1}{\sigma_\eta^2} [\nabla_{\mathbf{x}_k} \eta_k(\mathbf{x}_k)][\nabla_{\mathbf{x}_k} \eta_k(\mathbf{x}_k)]^T \right) p(\mathbf{x}_k) \, d\mathbf{x}_k.$$

Here, $P_\mathrm{D}^{\mathrm{RF}}$ and $P_\mathrm{D}^{\mathrm{EO}}$, $P_{\mathrm{FA}}^{\mathrm{RF}}$ and $P_{\mathrm{FA}}^{\mathrm{EO}}$, are the probabilities of detection and false alarm for the RF and EO sensors, respectively, and V_g^{RF} and V_g^{EO} are the corresponding validation volume regions. The *information reduction factor* scalars q^{EO} and q^{RF} represent the loss of information obtained from the measurements due to clutter and noise and thus result in a reduction in tracking performance. The information reduction factors vary between 0 and 1, depending on P_D, P_{FA}, and V_g [12]. Specifically, the larger P_D, the smaller P_{FA}, and the smaller validation region V_g will generate the larger q^{EO} and q^{RF}. Thus, we expect that improved detection performance will result in improved tracking performance. We also notice that the measurements covariance, σ_r^2, $\sigma_{\dot{r}}^2$, σ_θ^2, and σ_η^2, will also affect the PCRLB; smaller error in the measurements will yield higher tracking performance.

5.2. Waveform Design and Adaptive Control

Interpreting the PCRLB, we can obtain guidelines for waveform design for the RF-EO sensor parameter selection to improve tracking performance. Our aim using waveform design (for the RF sensor) and parameter selection (for the EO sensor) is to: (a) increase the probability of detection and decrease the validation regions for both the RF and EO sensors; and (b) decrease the measurement error covariance for the joint RF and EO processing. In this case, the range and range-rate measurement variances, $\sigma_r^2 = \nu_r^2/12$ and $\sigma_{\dot{r}}^2 = \nu_{\dot{r}}^2/12$, are proportional to range resolution ν_r and range-rate resolution $\nu_{\dot{r}}$, respectively. Also, $\nu_r = c/(2B)$, where B is the waveform bandwidth and $\nu_{\dot{r}} = (\lambda \, \mathrm{PRF})/(2N_{\mathrm{FFT}})$, where PRF

is the pulse repetition frequency, λ is the carrier frequency wavelength, and N_{FFT} is the length of the FFT used for the PD processing. Thus, we can control the range and range-rate resolution by varying the waveform's bandwidth, PRF, and carrier frequency. Similarly, the variance of the EO sensor measurements σ_θ^2 and σ_η^2 are proportional to the angle resolutions. Thus, improved EO sensor resolutions will lead to smaller measurement variances and thus to improved PCRLB. Note, however, that the range, range-rate and angle resolutions cannot be made arbitrary small as both sensors must maintain a large enough area for surveillance.

The joint RF-EO multi-target tracking problem can benefit from adaptive RF waveform design and EO sensor control. Specifically, multi-target tracking requires the RF sensors to maintain a large enough surveillance area to include all targets, while the range resolution is required to be small enough to provide accurate range measurements. As we need to consider limitations due to processing power in the overall system, there should be tradeoffs between the FOV and range resolution in designing the RF waveform, and similarly, between the FOV and angle resolution in adapting the EO control. Furthermore, as the RF sensors are distributed, they obtain different range-rate measurements from different aspects of the targets. The PRF should be low enough to minimize the range-rate measurement error but also high enough to guarantee that all the range-rates of all the targets are correctly measured. Thus, the tradeoff in the PRF depends on the motion characteristics of the targets. Note, also, that the waveform design and adaptive control will generate a reduced surveillance area for RF sensors (range and range-rate) and EO sensors (ground area). This will result in a smaller probability of false alarm that will further improve the detection performance.

A direct optimization of Equation (4) would lead to a WAMM design scheme. However, due to the computational complexity involved, inferences on a waveform design scheme were instead derived from the PCRLB. Specifically, at time step k, we obtain the target state estimate $\hat{\chi}_k$ using the RBPF and then use this estimate to predict the possible states at the next time step and the corresponding distributions using the target state models. Using the future target states, we then select sensor parameters. Specifically, we can select the waveform bandwidth to maintain a reasonably large range gate for all targets in the FOV while providing fine range resolution to reduce the measurement variance. For a waveform bandwidth between 5-150 MHz, a range resolution of 1 to 30 m can be obtained with a 100 m minimum (3 km maximum) range gate (in range bin 100). We can select the EO image resolution to maintain a reasonably large surveillance area while providing fine enough tracking resolution. For a 1,000-pixel 1-D EO image, the resolution varied between 10^{-5} and 10^{-3} rad, resulting in a 10 m minimum (1 km maximum) surveillance area. We can also select a high enough PRF to estimate the largest Doppler frequency, while providing fine resolution for slow-moving targets. For a 64 length FFT, the velocity resolution varied between 0.5 and 5 m/s, resulting in a 32 m/s minimum (320 m/s maximum) Doppler surveillance region.

6. NUMERICAL RESULTS AND DISCUSSION

We demonstrate the joint RF-EO multi-target tracking scenario in Fig. 1 in 2-D for simplicity. In our simulations, we used 4 RF-EO sensors to provide measurements to the data processing center alternatively, i.e., the RF sensors provide range and range-rate measurements at odd time instants and the EO sensors provide angle measurements at even time instants. At the first, 50th, 100th, and 150th time steps, target 1 2, 3, and 4 appear in the FOV, respectively. The targets are tracked using range measurements (dotted arcs), range-rate measurements (lines), and angle measurements (dotted lines).

The target tracking trajectories from a single simulation are shown in Fig. 2. As we can see, the trajectory begins with random selected positions (denoted by circles) and then follow the true trajectory. Note the false trajectory that originated due to false alarm measurements.
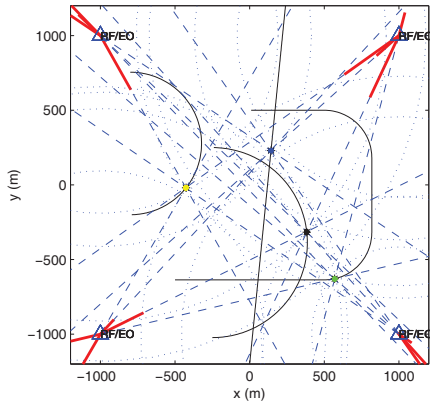

Fig. 1. Joint RF-EO multi-target tracking trajectory with 4 targets appearing at different points in the 2-D space: Target 1 (green circle) is (560,-631) m, Target 2 (blue circle) is at (114,240) m, Target 3 (black circle) is at (384,-327) m, and Target 4 (yellow circle) is at (-420,-11) m. The four RF-EO modes (blue triangles)are located at (1, 1) km, (-1, 1) km, (1, -1) km, and (-1, -1) km.
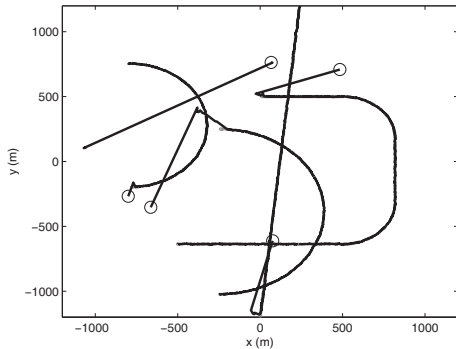

Fig. 2. Estimated tracking trajectories.

Fig. 3 shows the tracking mean-squared error (MSE) of the position estimate of the first target position using different numbers of RF-EO sensors, with and without waveform agility. As we can see, waveform agility substantially improves tracking performance for the single RF-EO sensor tracking case. The WAMM performance improvement is not as dramatic if a large number of RF-EO sensors is used as more measurement information is then available.

7. CONCLUSION

We investigated the joint multi-modal RF-EO multi-target tracking using adaptive waveform design and control. The Rao-Blackwellized particle filter was used to tracking an unknown number of targets while incorporating agility to the multi-modal tracking system to improve the overall tracking performance. The inference-based waveform design and adaptive control was successfully demonstrated using simulations. We are currently working towards finding a sub-optimal design solution based on the PCRLB.
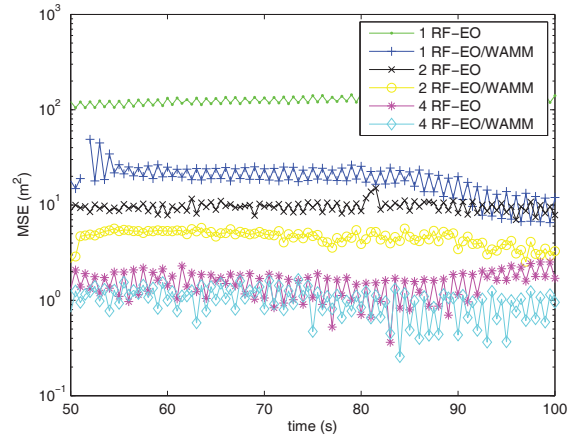

Fig. 3. MSE for multi-target tracking with an increasing number of RF-EO sensors. The MSE is demonstrated for one target only.

8. REFERENCES

[1] R. Chellappa, Q. Zheng, S. Kuttiked, S. Shekhar, and P. Burlina, "Site model construction for exploitation of EO and SAR images," in *RADIUS: IU for Imagery Intelligence*, O. Firschein, Ed., pp. 185–208. Morgan Kaufman, 1997.

[2] A. Theil, L. Kester, S. P. van den Broek, P. van Dorp, and R. van Sweeden, "FRESNEL program: Fusion of radar and electro-optical signals for surveillance on land," in *Society of Photo-Optical Instrumentation Engineers (SPIE) Conference Series*, I. Kadar, Ed., August 2001, vol. 4380, pp. 453–461.

[3] J. M. Blackaby, "Simultaneous RF/EO tracking and characterization of dismounts," M.S. thesis, Wright State Univ., 2008.

[4] E. Blasch and C. Yang, "Ten methods to fuse GMTI and HRRR measurements for joint tracking and identification," in *Int. Conf. Information Fusion*, Stockholm, Sweden, June 2004.

[5] M. E. Liggins, D. L. Hall, and J. Llinas, Eds., *Handbook Of Multisensor Data Fusion: Theory And Practice*, CRC Press, Boca Raton, FL, 2008.

[6] S. Sarkka, A. Vehtari, and J. Lampinen, "Rao-Blackwellized particle filter for multiple target tracking," *Information Fusion*, vol. 8, no. 1, pp. 2–15, 2007.

[7] C. Kreucher, K. Kastella, and A. O. Hero III, "Multitarget tracking using the joint multitarget probability density," *IEEE Transactions on Aerospace and Electronic Systems*, vol. 41, no. 4, pp. 1396–1414, October 2005.

[8] X. R. Li and V. P. Jilkov, "Survey of maneuvering target tracking, part I: Dynamic models," *IEEE Transactions on Aerospace and Electronic Systems*, vol. 39, pp. 1333–1364, October 2003.

[9] S. Blackman and R. Popoli, *Design and Analysis of Modern Tracking Systems*, Artech House Publ., New York, NY, 1999.

[10] J. Zhang, "Derivation of the PCRLB for joint RF-EO target tracking," http://papandreou.faculty.asu.edu/ Documents/Zhang_Rept_Sep09.pdf, June 2009.

[11] P. Tichavsky, C. H. Muravchik, and A. Nehorai, "Posterior Cramér-Rao bounds for discrete-time nonlinear filtering," *IEEE Trans. Signal Proc.*, vol. 46, pp. 1386–1396, May 1988.

[12] Y. Bar-Shalom and X.-R. Li, *Multitarget-multisensor Tracking: Principles and Techniques*, YBS Publ., 1995.